

Article

Catalytic Activity of Hybrid Iron Oxide Silver Nanoparticles in Methyl Methacrylate Polymerization

Sanaa M. Solyman ^{1,2,*}, Mohamed S.A. Darwish ^{1,3,*}  and Jungwon Yoon ³ ¹ Egyptian Petroleum Research Inst., 1 Ahmed El-Zomor St., El Zohour Region, Nasr City, Cairo 11727, Egypt² AL-Ghad International College for Applied Medical Sciences, Dammam 324XX, Saudi Arabia³ School of Integrated Technology, Gwangju Institute of Science and Technology, Gwangju 61005, Korea; jyoona@gist.ac.kr

* Correspondence: sanaa8763@hotmail.com (S.M.S.); msa.darwish@gmail.com (M.S.A.D.);

Tel.: +202-2274-7917 (S.M.S. & M.S.A.D.); Fax: +202-2274-7433 (S.M.S. & M.S.A.D.)

Received: 2 March 2020; Accepted: 6 April 2020; Published: 12 April 2020



Abstract: One of the challenges in the preparation of poly(methyl methacrylate) (PMMA) is to develop new catalytic systems with improved efficiency. A hybrid iron oxide silver catalyst holds promise in solving this issue. Catalysts were prepared at room temperature by a two-step technique. First, iron oxide nanoparticles were prepared by the reduction of FeCl₃ using sodium borohydride (NaBH₄) at room temperature. Second, magnetic nanoparticles doped with a series of Ag nanoparticles (Ag, Ag/3-aminopropyltriethoxysilane (APTES) and Ag/poly(ethyleneimine) (PEI)). The prepared catalysts were characterized using X-ray diffraction (XRD), transmission electron microscopy (TEM), dynamic light scattering (DLS), scanning electron microscopy/energy dispersive X-ray spectroscopy (SEM/EDX), and Fourier-transform infrared spectroscopy (FTIR). The catalytic activity of Fe, Ag/Fe, PEI-Ag/Fe, and APTES-Ag/Fe in methyl methacrylate (MMA) polymerization was investigated in the presence of O₂, N₂, NaHSO₃, and benzoyl peroxide in bulk or solution conditions. The produced polymer was characterized by gel permeation chromatography (GPC) and proton nuclear magnetic resonance spectroscopy (¹H NMR). The structures of PEI-Ag/Fe and APTES-Ag/Fe are assumed. The conversion efficiency was 100%, 100%, 97.6%, and 99.1% using Fe, Ag/Fe, PEI-Ag/Fe, and APTES-Ag/Fe catalysts at the optimum conditions, respectively. Hybrid iron oxide silver nanoparticles are promising catalysts for PMMA preparation.

Keywords: hybrid structure catalysts; iron/silver/organic; PMMA; polymerization

1. Introduction

Polymethyl methacrylate (PMMA) is a thermoplastic that is transparent with resistance to UV and has been used in a wide range of fields and applications. PMMA is versatile and is used in automotive, construction, electronics, and medical applications [1–5]. One of the challenges in the preparation of PMMA is the efficiency of conversion [6,7]. Polymerization of MMA has been achieved by different techniques such as bulk and solution polymerization, and different mechanisms such as free radical, living free radical, anionic, and redox mechanisms [8–14]. In the presence of two metallocenes, the rate of the MMA polymerization at the initial stages of conversion (5%–10%) increases strongly, as compared with that of the benzoyl peroxide and the zirconocene-benzoyl peroxide systems [6]. The free radical copolymerization of methyl methacrylate/methacrylic acid (poly(MMA-co-MAA) copolymer) was investigated using benzoyl peroxide initiator and ferrocene as an accelerator at 60 °C. It was found that more yield with high conversion (84.78%) are obtained when copolymerization occurs in the presence of ferrocene [7]. Copper phthalocyanine (CuPc) supported over bentonite is relatively more specific than Nickel phthalocyanine (NiPc) in the polymerization of MMA in terms

of conversion yield (viz, 63.63% for CuPc and 46.55% for NiPc) [8]. Free radical polymerization systems mainly rely on the amine/peroxide redox reaction to generate the polymerization initiating radicals upon mixing of the two components [9–14]. Tertiary aromatic amines have been used with benzoyl peroxide (BPO) to form an effective initiation system in the free-radical polymerization of acrylic resins, especially that of methyl methacrylate (MMA) [14]. The kinetics of the free radical bulk polymerization of methyl methacrylate (MMA) was studied using the benzoyl peroxide (BPO)/amine initiation system. It was found that the maximum rate occurs when the ratio of [BPO]/[amine] is approximately equal to 1.5 [9]. The demand for catalysts with particular and specific physicochemical properties is constantly increasing. The integration of the unique properties of inorganic and organic nanoparticles in the same structure results in new properties that can be used in various applications. Hybrid inorganic/organic nanoparticles have gained particular attention because of fundamental scientific interest in various cutting-edge technological applications of these species, including their use in sensors [15], nanomedicine [16], antibacterial activity [17,18], magnetic resonance imaging (MRI) [19], hyperthermia [20], and catalysis [21,22]. It is widely known that the presence of a second co-metal can improve the properties of the catalytic system [23]. Catalysts based on magnetic silver nanoparticles have been attempted for the design of hybrid nanostructures that combine the physical and chemical properties of each component [23]. The catalyst with magnetic character provides: (1) easier separation of catalyst samples from the solution using an external magnet, (2) recovery of properties with cost-effectiveness, (3) re-dispersal under magnetic field, and (4) non-toxicity [24,25]. The presence of silver nanoparticles in the magnetic catalyst structure increases its catalytic activity as a heterogeneous catalyst [26,27]. Catalysts with the enhanced chemical and physical properties make the hybrid nanostructures suitable research targets in different applications [28–32]. The catalytic oxidation of volatile organic compounds (VOCs) has been carried out using the nanostructure catalyst of Fe–Ag–ZSM-5 [28]. Fe@Ag nanoparticle with calcium alginate beads was prepared for the reduction of nitrophenols [29]. Ag@Fe₂O₃ catalyst was prepared for the removal of 2-propanol [30]. Ag/Fe₂O₃ activity in the low-temperature oxidation of CO was studied [31]. Also, the catalytic application of Ag–Fe₂O₃–carbon nanocomposites was investigated [32]. Nanocomposites based on hybrid iron oxide silver have recently emerged as promising catalysts, where the shell not only protects the core from oxidation but also facilitates surface modification and functionalization to overcome problems caused by oxidation and aggregation of iron oxide nanoparticles (IONPs) [29,30]. Many methods have been used to prepare magnetic silver nanoparticles, such as hydrothermal decomposition [33], thermal decomposition [34], and two-step chemical method [35]. The efficiency of generation of the polymerization initiating radicals in MMA polymerization depending on the ratio of amine/peroxide has been studied [9–14]. In our study, APTES and PEI were used as sources of mono and multi amine groups, respectively. In the MMA polymerization reaction, naked magnetic silver nanoparticles and those coated with APTES and PEI were investigated to measure their efficiency in generating the polymerization initiating radicals. To the best of our knowledge, catalyst based on magnetic nanoparticles doped by silver has not yet been prepared at room temperature for bulk and solution polymerization of MMA. In this work, magnetic nanoparticles doped by silver catalysts were prepared in an open system at room temperature through the two-step reduction technique. The prepared samples of synthesized Fe, Ag/Fe, APTES–Ag/Fe, and PEI–Ag/Fe nanoparticles were analyzed by X-ray diffraction (XRD), transmission electron microscopy (TEM), dynamic light scattering (DLS), scanning electron microscopy/energy dispersive X-ray spectroscopy (SEM/EDX), and Fourier-transform infrared spectroscopy (FTIR). Their catalytic efficiency was investigated as a new family of nanocomposites that may be appropriate for MMA polymerization.

2. Results and Discussion

2.1. Catalyst Preparation

In this work, magnetic nanoparticles doped by silver catalyst based on Ag/Fe, APTES–Ag/Fe, and PEI–Ag/Fe were prepared in an open system at room temperature using the two step reduction technique, as shown in Figure 1. First, the iron oxide nanoparticles were prepared by the reduction of FeCl_3 using sodium borohydride (NaBH_4) at room temperature. Second, magnetic nanoparticles doped with a series of Ag nanoparticles (Ag, Ag/3–amino propyltriethoxysilane (APTES), and Ag/poly(ethyleneimine) (PEI)).

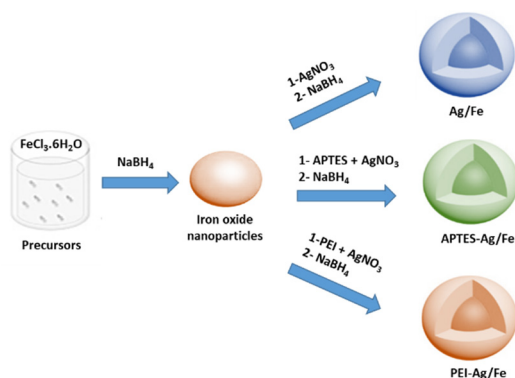


Figure 1. Illustrated scheme for the preparation of catalysts Ag/Fe, 3-amino propyltriethoxysilane (APTES)-Ag/Fe, and poly(ethyleneimine) (PEI)-Ag/Fe by a two-step reduction process.

2.2. Catalyst Characterization

2.2.1. XRD

The phase identification of the prepared nanoparticles was investigated using XRD. Figure 2 displays the XRD patterns of: (a) iron oxide nanoparticles (Fe), (b) silver/iron (Ag/Fe), (c) APTES–Ag/Fe, and (d) PEI–Ag/Fe. Figure 2a shows the XRD patterns of the prepared nanoparticles. The two weak peaks visible at the 2θ of 45° and 35° indicate the presence of both zero-valent iron and iron oxide crystalline phases, respectively [36]. Formation of iron oxide nanoparticles occurs as a result of using water in the medium without an inert gas and using water in the washing of the produced nanoparticles. ZVI nanoparticles naturally oxidize upon reaction with water and oxygen and form an iron oxide layer on the surface, which has been noticed and confirmed previously [36–39]. Recently, Mukhtar et al. stated that with the increase of reaction time in water from 0 to 360 min, the oxide layer thickness increases from 2.5 to 10 nm. The composition and phase of the oxide layer formed on an iron core depends on the distance from the inner Fe core to the outer oxide layers, i.e., usually there is a progression from zero valent $\text{Fe} \rightarrow \text{FeO} \rightarrow \text{Fe}_3\text{O}_4 \rightarrow \text{Fe}_2\text{O}_3$. Although, for room temperature oxidation, a very thin oxide layer is formed, which makes it hard to differentiate the spatial variation of oxide shells [39]. Figure 2b shows that four characteristic peaks appeared at 2θ values of 38° , 44° , 64° , and 77° , which correspond respectively to the (111), (200), (220), and (311) lattice planes of the face-centered cubic phase (FCC) of Ag, (JCPDS No. 03-0931) [17]. Silver lattice plane (200) mostly overlapped with the Fe lattice plane (110) in the Ag/Fe spectrum. In Figure 2c, the intensity of Ag lines decreased due to the assembling of APTES–Ag with Fe. This observation may indicate the dispersion and interaction of Ag nanoparticles with APTES molecules. In the spectrum of PEI–Ag/Fe, shown in Figure 2d, shifting in peak position towards lower 2θ of 35.41° and 63.29° with decreasing intensities of peaks is caused by the presence of PEI molecules in the structure of magnetic nanoparticles (MNPs) [40].

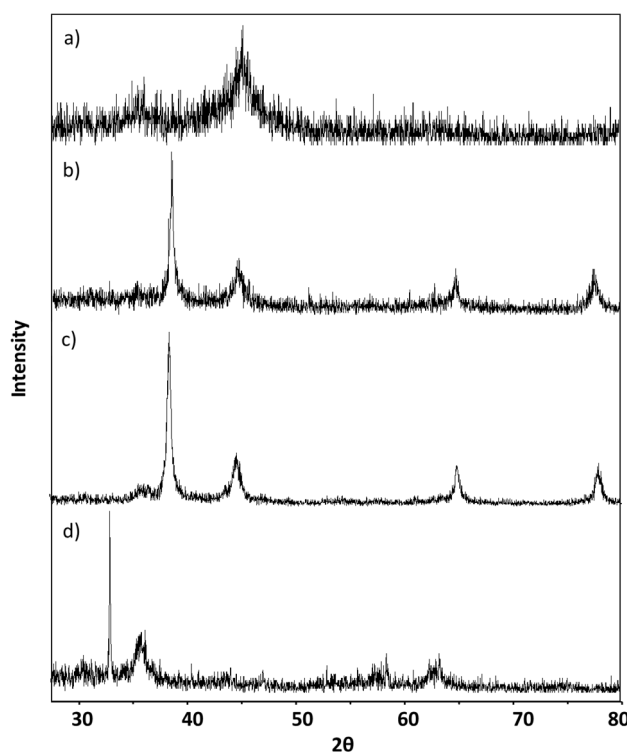


Figure 2. X-ray diffraction (XRD) patterns of: (a) synthesized Fe, (b) Ag/Fe, (c) APTES–Ag/Fe, and (d) PEI–Ag/Fe.

2.2.2. Scanning Electron Microscope and EDX

The morphology of the prepared Fe, Ag/Fe, APTES–Ag/Fe, and PEI–Ag/Fe nanoparticles and their elemental analysis were investigated using SEM and EDX, and are shown in Figure 3. SEM of Fe shows spinal and plate-like morphology and its EDX show the presence of Fe and O. The EDX of Ag/Fe confirms the presence of Fe, Ag, and O. On the other hand, its SEM shows ordered and homogeneous aggregates like roses. Each one appearing as agglomerated nanoplates (mostly Ag around Fe nanoparticles). Also EDX analysis of APTES–Ag/Fe and PEI–Ag/Fe confirm the presence of Fe, Ag, and O in both samples. The morphology of PEI–Ag/Fe appears as large agglomerated particles, which is further confirmed with TEM and DLS.

2.2.3. TEM

The transmission electron microscope (TEM) images of Ag/Fe, APTES–Ag/Fe, and PEI–Ag/Fe nanoparticles are shown in Figure 4. It shows the magnetic nanoparticles doped by silver with a particle size of ~20 nm. It was observed that the presence of APTES–Ag decreases the aggregation between the prepared nanoparticles. APTES–Ag/Fe shows less aggregation, which is further confirmed by narrow size distribution observed using DLS. In contrast, PEI–Ag/Fe shows high aggregation, which is further confirmed by a wide size distribution observed using DLS.

2.2.4. The Hydrodynamic Size of Catalyst Samples

The hydrodynamic sizes of Fe, Ag/Fe, APTES–Ag/Fe, and PEI–Ag/Fe were measured using the Dynamic Light Scattering (DLS) technique, as shown in Figure 5a–d, respectively. DLS revealed that the prepared iron oxide nanoparticles have an average particle size of 39 nm with a narrow distribution. This value was increased by the addition of Ag nanoparticles and the assembling of APTES–Ag and PEI–Ag on to the Fe surface, as shown in Figure 5b–d. The mean hydrodynamic sizes were 195.8 nm, 295.3 nm, and 283.5 nm for Ag/Fe, APTES–Ag/Fe, and PEI–Ag/Fe, respectively. These results concur with the SEM photos that show agglomerated nanocomposite particles in each sample.

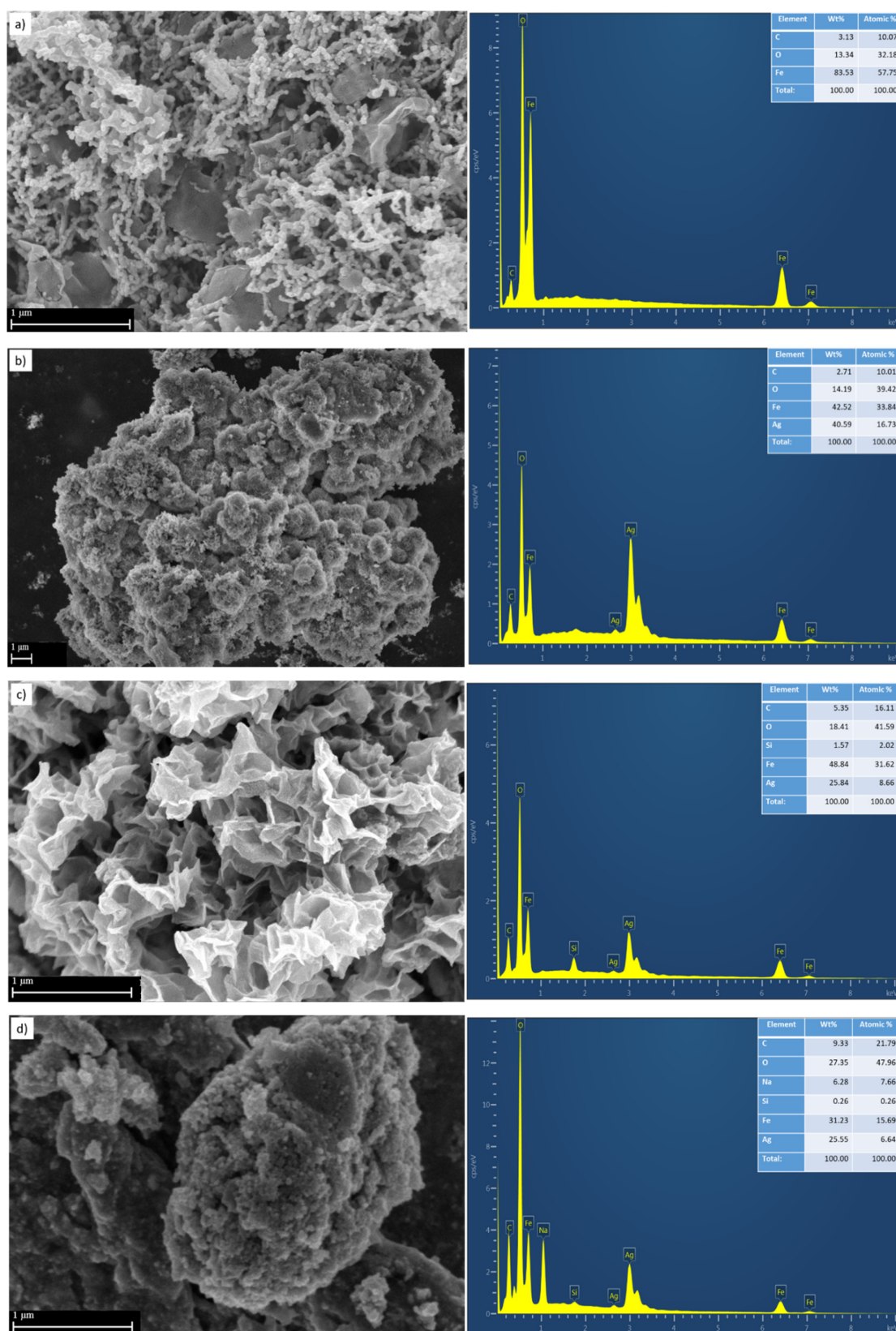


Figure 3. Scanning electron microscopy (SEM) micrographs and the elemental analysis using energy dispersive X-ray spectroscopy (EDX) of (a) synthesized Fe, (b) Ag/Fe, (c) APTES-Ag/Fe, and (d) PEI-Ag/Fe.

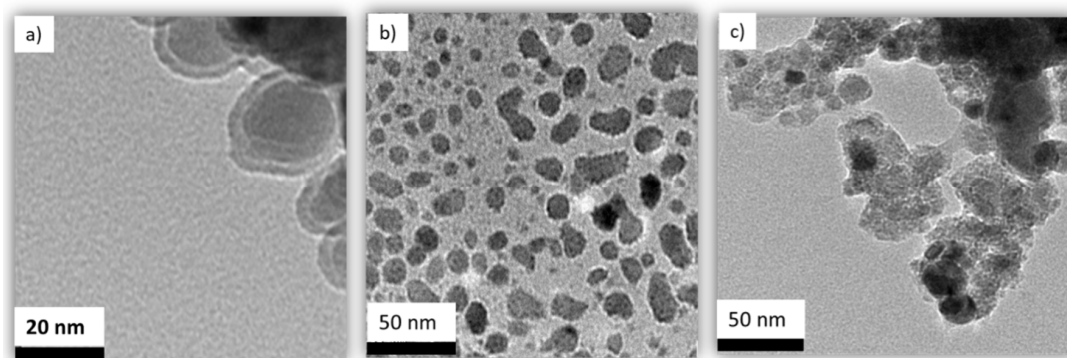


Figure 4. The transmission electron microscopy (TEM) micrographs of (a) Ag/Fe, (b) APTES-Ag/Fe, and (c) PEI-Ag/Fe.

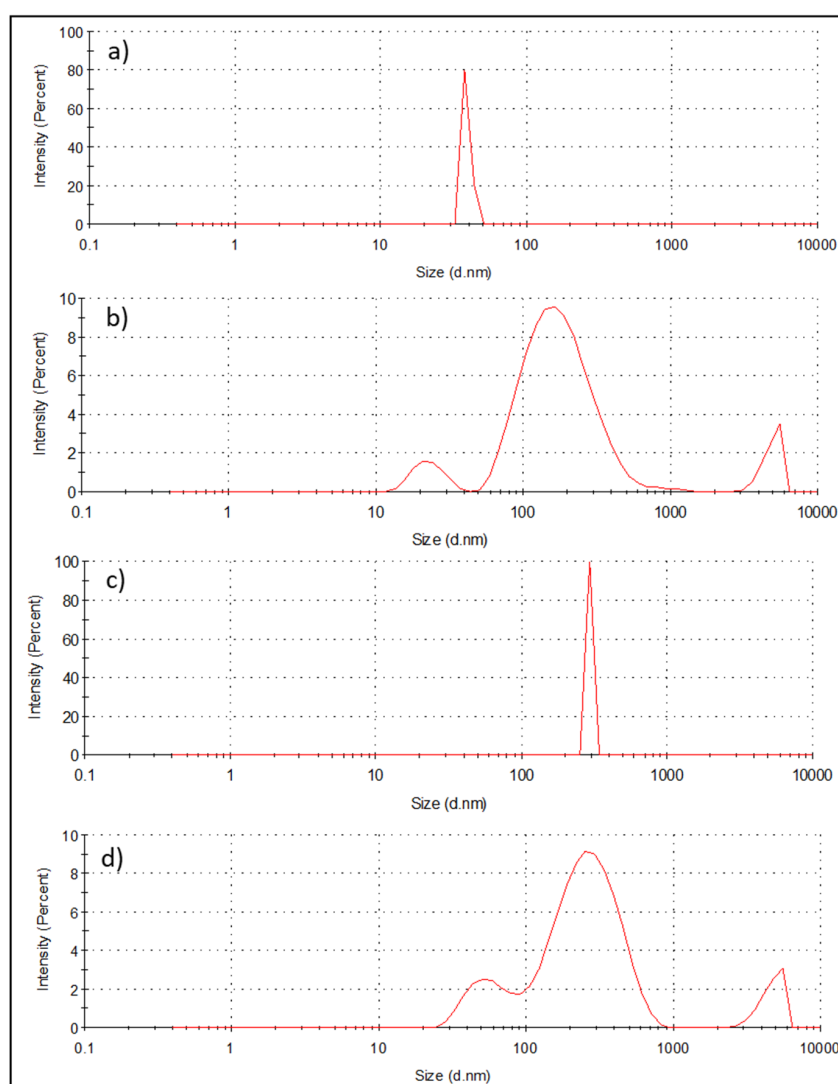


Figure 5. The particle size distribution measured using Dynamic Light Scattering (DLS) of (a) synthesized Fe, (b) Ag/Fe (c), APTES-Ag/Fe, and (d) PEI-Ag/Fe.

DLS provides statistical representative data about the hydrodynamic size of nanomaterials (hydrodynamic radius on an ensemble average). However, the interpretation of DLS data involves the interplay of a few parameters, such as the size, concentration, shape, polydispersity, and surface properties of the MNPs [41–44]. If the sample is too dilute, there may not be enough scattering

events to make a proper measurement. On the other hand, if the sample is too concentrated, then multiple scattering can occur. Moreover, at high concentrations, the particles might not be freely mobile with the spatial displacement driven solely by Brownian motion. The displacements may be strongly influenced by particle interactions. This scenario is especially true in case of MNPs with interparticle magnetic dipole–dipole interactions. Although DLS can sometimes measure anisotropic nanostructures, it generally assumes spherical shaped particles. Overall, the real-time screening of NPs by DLS provides important insights into their aggregation process as it quantitatively measures the size of the particle clusters thus formed.

2.2.5. FT-IR

Functional groups on the surface of the magnetic nanoparticles doped by silver were detected by FT-IR in Figure 6. The absorption peak near to 500 cm^{-1} confirms the presence of a Fe–O bond, which related to the iron oxide nanoparticles. The peak closes to 800 cm^{-1} is due to Si–O and implies the presence of APTES. The absorption contribution from the free $-\text{NH}_2$ group of APTES observed at 3400 cm^{-1} . The absorption bands near to 3400 and 1100 cm^{-1} account for the vibration bands of NH_2 and C–N respectively were given to PEI. The determined peaks point to the existence of APTES and PEI on the surface of nanoparticles.

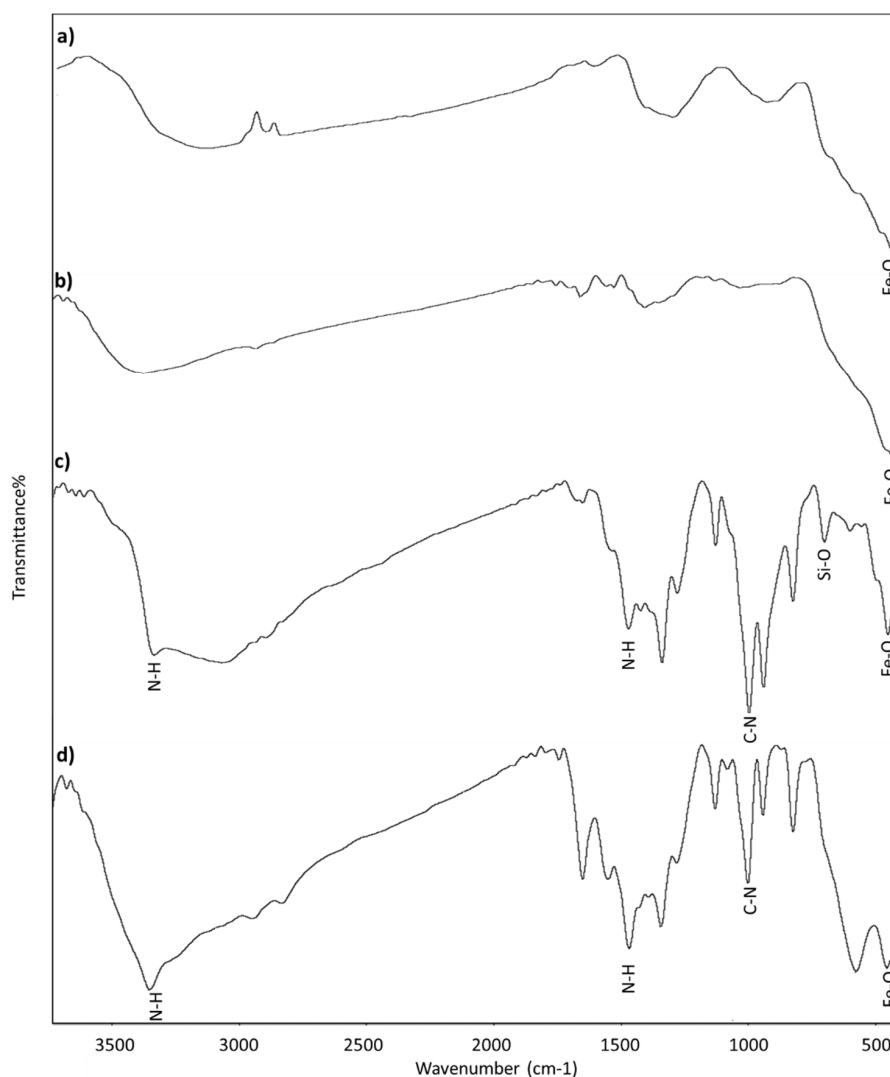


Figure 6. Fourier-transform infrared spectroscopy (FT-IR) of (a) synthesized Fe, (b) Ag/Fe, (c) APTES-Ag/Fe, and (d) PEI-Ag/Fe.

2.3. The Catalytic Activity of Different Catalyst Samples in MMA Polymerization

Table 1 displays the conversion percentage (Conv.%) of PMMA using different catalyst samples under different conditions: (A) Bulk polymerization in O₂ or N₂ atmosphere for 5 h with and without NaHSO₃, and (B) solution polymerization in acetonitrile (AcN) with and without benzoyl peroxide (B.P) in O₂ atmosphere (Catalyst/B.P ratio is 3/1 and 4/1) after reaction times of 3 and 5 h, respectively, with a reaction temperature of 80 °C.

(A) All catalyst samples have nil activity in bulk polymerization of MMA in O₂ atmosphere. This result indicates that O₂ has an inhibition effect on these catalysts. According to Hurvois et al. [45], this may be due to the blocking of the active sites and prevention of the formation of active species. Also, it is nil in N₂ atmosphere except for PEI–Ag/Fe sample that gave 4% PMMA as shown in Table 1. This result is mostly due to NH₂ groups of PEI which undergo initiation by hydrogen transfer to MMA double bond (Cat–HN^{δ-} ... [^{δ+}CH₂–C^{δ-}(H^{δ+})(CH₃)(COOCH₃)–] and the polymerization proceeds by anionic mechanism [46,47]. Other catalyst samples are inactive without a cocatalyst or initiator at these conditions. On the other hand, the addition of NaHSO₃ initiated the bulk polymerization reaction in N₂ atmosphere with all catalyst samples which proceeded mostly by the redox mechanism [48]. The conversion (%) was 1.5%, 16.7%, 40%, and 42.3% using Fe, Ag/Fe, PEI–Ag/Fe, and APTES–Ag/Fe, respectively. According to previous studies [8], HSO₃⁻ can work as a reducing agent, H-donor, a chain transfer agent, and a cocatalyst. Iron with/without silver as a transition metal forms a redox system with NaHSO₃ according to different studies [48]. That is because HSO₃⁻ reduces the transition metal and produces SO₃⁻ which starts the initiation and propagation steps of MMA as shown in Equation (1):

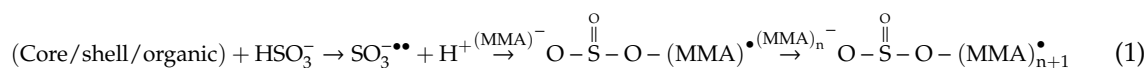


Table 1. The conversion% of PMMA using different catalyst samples at 80 °C and different conditions, Bulk polymerization in O₂ and N₂ atmosphere for 5 h with and without NaHSO₃ and solution polymerization in AcN + B.P in O₂ gas with catalyst/B.P ratio = 3/1 and 4/1 after reaction times of 3 and 5 h.

Catalyst Samples	Bulk, O ₂	Bulk, N ₂	Bulk, N ₂ , NaHSO ₃	1mL of	1mL of	1mL of
				(AcN+B.P), O ₂ , Cat., Cat.: B.P (3:1), 3 h	(AcN+B.P), O ₂ , Cat., Cat.: B.P (4:1), 3 h	(AcN+B.P), O ₂ , Cat., Cat.: B.P (4:1), 5 h
Fe	Nil	Nil	1.5	34.0	45.2	88.6
Ag/Fe	Nil	Nil	16.7	46.7	75.5	100.0
PEI–Ag/Fe	Nil	4.0	40.0	81.4	88.2	97.0
APTES–Ag/Fe	Nil	Nil	42.3	70.0	81.7	95.0

Also, assembling of Ag on to the Fe surface enhances the redox process and the polymerization activity increases from 1.5% to 16.7% using Fe and Ag/Fe, respectively. This may indicate that AgNPs shell interacted with Fe nanoparticles due to the electron plasmon resonance of silver and the electron deficiency of Fe in the Ag/Fe sample. As a result, new stronger active sites and more free radicals are created, resulting in higher activity. These results reflect the high performance of Ag as a further activator in the presence of HSO₃⁻. Also, the performance of catalyst samples increases by seeding of AgNPs on PEI or APTES and their assembling on to the Fe surface, and so the conv.% increases to 40% and 42.7%, respectively, as shown in Table 1. It is concluded that in bulk polymerization of MMA, all catalyst samples are inhibited in oxygen but activated using NaHSO₃. The results also reflect the high performance of Ag NPs as an activator or cocatalyst.

(B) Similar to the bulk process, the results of solution polymerization in AcN presented in Table 1 indicate nil activity using all catalyst samples in O₂ atmosphere. These results confirm the inhibition

effect of oxygen with these catalyst samples at these conditions. In light of previous publications, we postulated that the studied catalyst samples may have the behavior of a ferrocene-benzoyl peroxide-oxygen system due to the effect of magnetic iron [49–53]. So, benzoyl peroxide solution in acetonitrile (0.1 mL, 1% *w/v*) was added with different catalyst/ benzoyl peroxide ratios (Cat./B.P = 3/1 and 4/1) for 3 h in oxygen atmosphere at the same reaction temperature (80 °C). The Conv.% increased due to the addition of B.P with Cat./B.P ratio 3/1 and more improvement was obtained by increasing this ratio to 4/1, as shown in Table 1. Also, longer reaction time (5 h) using the optimum ratio (4/1) produced higher polymer yields (88.6, 100, 97 and 95%) using the catalyst samples (Fe, Ag/Fe, PEI–Ag/Fe, and APTES–Ag/Fe), respectively. Table 2 introduces the molecular weight distribution results \overline{M}_w , \overline{M}_n , and polydispersity index of PMMA which was produced using the studied benzoyl peroxide-oxygen catalyst system in the solution polymerization process at different Cat./B.P ratios after 3h at 80 °C. The results reveal that \overline{M}_w and \overline{M}_n values (from Table 2) and also the Conv.% (from Table 1) of PMMA was increased by increasing the Cat./B.P ratio from 3/1 to 4/1 with all catalyst samples except the Ag/Fe sample, with which the \overline{M}_w and \overline{M}_n decreased even though the conv.% increased from 46.7 to 75.5%. It can be concluded that increasing the Cat./B.P ratio resulted in increases in the number of active sites, the decomposition of B.P and the number of free radicals. Also, the chain transferring rate increased mostly due to AgNPs in Ag/Fe sample relative to the propagation rate, this resulted in increased conv.% with decreased \overline{M}_w and \overline{M}_n while using the 4/1 ratio. The polydispersity index ranged between 2.19 and 2.96 indicating a broadly distributed polymer.

Table 2. Gel permeation chromatography (GPC) analysis of poly(methyl methacrylate) (PMMA) produced by solution polymerization using Cat./B.P = 3/1 and 4/1 at 80 °C for 3 h in an oxygen atmosphere.

Catalyst Samples	Fe 3/1	Fe 4/1	Ag/Fe 3/1	Ag/Fe 4/1	PEI–Ag/Fe 3/1	PEI–Ag/Fe 4/1	APTES–Ag/Fe 3/1	APTES–Ag/Fe 4/1
$\overline{M}_w \times 10^{-3}$	174	190	266	239	262	233	176	195
$\overline{M}_n \times 10^{-3}$	66	86	107	100	89	95	66	74
$\overline{M}_w / \overline{M}_n$	2.62	2.19	2.48	2.39	2.96	2.45	2.65	2.62

Table 3 presents the Conv.%, molecular weight distribution results, tacticity%, β , and α values of PMMA prepared by solution polymerization at 80 °C for 3 h in an oxygen atmosphere using iron-based catalyst systems and benzoyl peroxide with catalyst/B.P ratio of 4/1. The weight average molecular weight (\overline{M}_w) of PMMA increased from 190×10^{-3} to $(239 \text{ and } 233) \times 10^{-3}$ using Fe, Ag/Fe, and PEI–Ag/Fe, and then decreased to 195×10^{-3} using APTES–Ag/Fe. The polydispersity index ($\overline{M}_w / \overline{M}_n$) was 2.19 using the Fe sample, which then increased to 2.39, 2.45, and 2.62 using other samples, as shown in Table 3. The polydispersity index values are higher than the range for a living polymerization process ($\overline{M}_w / \overline{M}_n = 1.1\text{--}1.5$), postulating broadly distributed polymer chains [49]. Besides, ^1H NMR tacticity% (mm, rm, and rr), β and α values show a disappearing isotactic polymer and so β value is zero due to assembling of AgNPs in Ag/Fe sample, as shown in Table 3. These results confirm that the Ag/Fe catalyst may work with a different addition mechanism which results in the disappearance of the isotactic chain. The tacticity% of I(mm):H(rm):S(rr) shows that the syndiotactic polymer chains (rr) are higher than 50% in all the catalyst samples, thus indicating a free radical mechanism [8]. Also, β values ($4[\text{mm}] / [\text{rr}]^2$) of the polymer produced by other assembled samples that contain AgNPs are close to 1, 1.18 (PEI–Ag/Fe), and 1.16 (APTES–Ag/Fe) indicating that AgNPs form the most important active sites which result in a chain-end control mechanism. Using the all indicating no enantiomorphic site-control approach, the values of α ($2[\text{rr}] / [\text{mr}]$) are found to be far from 1. The building of PEI–Ag/Fe and APTES–Ag/Fe samples results in improvement of the

Conv.% of PMMA of 97% and 95%, respectively, relative to Fe and Ag/Fe samples. APTES–Ag/Fe produced a lower number of active sites relative to PEI–Ag/Fe because PMMA has lower \overline{M}_w and \overline{M}_n and slightly lower Conv.%.

Table 3. Results of methyl methacrylate solution polymerization at 80 °C for 3 h in an oxygen atmosphere using iron-based catalyst samples and benzoyl peroxide as cocatalyst (Cat./B.P = 4/1). The table shows the conversion%, the molecular weight distribution, and ^1H NMR results of PMMA.

Catalyst Samples	Conv.%	$\overline{M}_{ww} \cdot 10^{-3}$	$\overline{M}_w/\overline{M}_n$	Tactospecificity%			β	A
				I(mm)	H(rm)	S(rr)		
Fe	45.2	190	2.19	8.7	29.0	62.3	2.57	4.3
Ag/Fe	75.5	239	2.39	0.0	42.5	57.5	0.0	2.7
PEI–Ag/Fe	88.2	233	2.45	9.2	39.8	51.0	1.18	2.6
APTES–Ag/Fe	81.7	195	2.62	6.2	35.3	58.5	1.16	3.33

The abovementioned results and other studies indicated that the presented catalyst samples mostly have ferrocene like mechanism [49–53]. To confirm this idea and to compare with previously studied ferrocene systems, the polymerization reaction was repeated with the last optimum conditions (Cat./B.P = 4/1 and 5 h) but without oxygen. In this reaction, the conv.% increased to 100%, 100%, 97.6%, and 99.1% using Fe, Ag/Fe, PEI–Ag/Fe, and APTES–Ag/Fe, respectively. The polymerization process was almost complete, which confirms the ability of Fe based samples to react with B.P and produce benzoate which catalyzes B.P decomposition to free radicals [50]. This resulted in accelerating the propagation nearly without termination. The polymerization process is mostly via free radical mechanism with/without oxygen.

The role of the ferrocenium radical cation and the $\text{Cp}_2\text{Fe}^+-\text{O}^\bullet$ radical in the initiation of methyl methacrylate polymerization in the absence and presence of oxygen was studied in [49]. They found that the polymerization of MMA proceeds in the presence of ferrocene and BP under both anaerobic and aerobic conditions and the rate is higher in the presence of oxygen. Also, the more efficient ratio of ferrocene/benzoyl peroxide is 4:1. The reactivity of ferrocenium cations with molecular oxygen in polar organic solvents was investigated in [45]. When the solvent is non-oxidizable, such as acetonitrile, the oxygen decomposes the active specie (ferrocenium cation) to ferrocene. However, in oxidizable solvents, such as dimethylformamide (DMF), the ferrocenium cation reversibly forms peroxy radical cations. Ferrocene-benzoyl peroxide system, which is mostly used in an inert environment, is capable of forming active species in the presence of oxygen as an initiator of vinyl monomer polymerization [52].

A comparison between ferrocene and our Fe-based system that we postulate as (Fe samples-benzoyl peroxide) having a ferrocene mechanism is presented as follows: (1) Ferrocenium cation (the active species) decomposed to ferrocene in an oxygen atmosphere in the acetonitrile solvent, meaning that it is inhibited at these conditions and our Fe-based catalyst samples have nil activity in bulk and solution conditions [45]. (2) Ferrocene accelerates benzoyl peroxide decomposition producing free radicals that are necessary to initiate the reaction according to previous publications [49–53]. Our samples with benzoyl peroxide produce free radicals that improved the conv.%. (3) Ferrocene-benzoyl peroxide works with and without oxygen but in oxygen it is better [49]. Our Fe-based samples-benzoyl peroxide worked with and without oxygen but without oxygen it was better. Finally, the optimum conditions for MMA polymerization using the studied catalyst samples are Cat./B.P = 4/1, for 5 h and without O_2 in AcN solvent by solution technique.

3. Experimental Work

3.1. Materials

Ferric chloride hexahydrate ($\text{FeCl}_3 \cdot 6\text{H}_2\text{O}$), silver nitrate (AgNO_3), sodium borohydride (NaBH_4), 3-aminopropyltriethoxysilane (APTES), poly(ethyleneimine) solution (PEI) ~50% in H_2O (M.W.

600,000–1,000,000), NaHSO₃, benzoylperoxide, and methyl methacrylate (MMA) were all obtained from Sigma–Aldrich, Germany.

3.2. Preparation of Iron Oxide Nanoparticles

The iron oxide nanoparticles were prepared using the reduction process. 0.55 g of FeCl₃·6H₂O was dissolved in a mixture of ethanol 24 mL and deionized water (DI water) 6 mL at room temperature. NaBH₄ (0.3783 g in 100 mL water) was added dropwise to the solution in an open system (without inert gas) with higher stirring using mechanical stirrer for 15 min. The final nanoparticles precipitate was filtered, washed with DI water, and then dried under vacuum and denoted as (Fe).

3.3. Preparation of Catalysts Based on Magnetic Nanoparticle Doped by Silver

Three types of catalysts based on magnetic nanoparticles doped by silver were prepared using the reduction method.

- Unmodified catalyst based on silver/iron oxide was prepared by the addition of AgNO₃ (0.170 g in 100 mL DI water) to the iron oxide nanoparticles (0.5 g), which were prepared in the first step. AgNO₃ was reduced by the dropwise addition of NaBH₄ (0.3783 g in 100 mL water) at room temperature in an open system (without inert gas) with higher stirring using mechanical stirrer for 15 min. The final precipitate was filtered, washed with DI water, and then dried under vacuum. This sample was denoted as Ag/Fe.
- Preparation of organic-silver/iron oxide catalyst based on APTES–Ag/Fe was carried out by the addition of AgNO₃ solution (0.17 g in 100 mL DI water) and 4 g of APTES to the prepared iron nanoparticles (0.5 g). AgNO₃ was reduced using the same abovementioned method. The final precipitates were filtered, washed with DI water, and then dried under vacuum. This sample was denoted as APTES–Ag/Fe.
- Preparation of polymer-silver/iron oxide catalyst based on PEI–Ag/Fe was carried out by the addition of AgNO₃ solution (0.17 g in 100 mL DI water) and 4 g of PEI to the prepared iron nanoparticles (0.5 g). AgNO₃ was reduced using the same abovementioned method. The final precipitates were filtered, washed with DI water, and then dried under vacuum. This sample was denoted as PEI–Ag/Fe.

3.4. Catalyst Characterization

Different techniques have been used for the characterization of the prepared catalyst samples. X-ray diffraction (XRD) of the nanoparticles was analyzed using an X-ray diffractometer (Rigaku, Japan) equipped with a copper X-ray tube and Cu KR radiation. Measurement was performed at a scan speed of 4°/min with a 2θ ranging from 4° to 80°.

Microscopy images and elemental analysis of all catalyst samples were achieved by scanning electron microscopy (SEM) and energy dispersive X-Rays spectroscopy (EDX) using a Zeiss ULTRA Plus field-emission SEM equipped with a Schottky cathode. The images of catalyst samples were analyzed through Smart SEM software v5.05 (Zeiss, Germany) for imaging run at 1.5 kV.

Transmission electron microscopy images (TEM) were obtained using a JEOL JEM-1230 working at 120 kV with an attached CCD camera to investigate the nanostructure of the prepared catalyst samples. Dynamic Light Scattering (DLS) analysis was employed to measure the hydrodynamic diameters of nanoparticles aggregates in DI water using a Zetasizer Nano DLS unit (Malvern Instruments). Fourier transform infrared spectroscopy (FT–IR) was performed using the Tensor 27 Infrared Spectrometer (Bruker, USA).

3.5. Methyl Methacrylate Polymerization Reaction

The catalytic activity of Fe, Ag/Fe, PEI–Ag/Fe and APTES–Ag/Fe was studied through bulk and solution polymerization of MMA.

- Bulk polymerization was performed by injecting 1.4 g of freshly cleaned MMA and 0.03 g of the catalyst sample into the reaction test tube (capacity 20 mL). The efficiency of the catalyst samples is tested by: (1) the passing of dry and pure N₂ to test the catalyst behavior only without an initiator; (2) passing pure and dry O₂ gas to test the activity of the catalysts with oxygen as the initiator; and (3) passing of N₂ with the addition of 0.1 mL of NaHSO₃ saturated solution to test the catalyst activity in the presence of sodium hydrogen sulfite [8]. The reaction time was 5 h in all bulk experiments.
- Solution polymerization was performed by adding 1.4 g MMA and 0.03 g catalyst in 1 mL of acetonitrile solvent (AcN). The catalytic activity of catalysts was evaluated by different experiments: (1) passing O₂ as the initiator; (2) adding 1 mL of benzoyl peroxide (B.P) solution as the co-initiator plus passing oxygen; (3) using specific catalyst/benzoyl peroxide ratios of 3/1 and 4/1 w/w, by respectively dissolving 0.075 or 0.1 g of benzoyl peroxide in 10 mL of AcN and taking 1 mL of the solution and adding it to the reaction mixture; and (4) the reaction time was varied as 3 and 5 h.

The test tube was sealed off during all the bulk and solution experiments and placed at 80 °C in a thermo-stated water bath. Once the reaction time was complete, the reaction mixture tube was cooled to room temperature, carefully opened, and the PMMA was separated from the catalyst using a previously published method [8].

PMMA conversion (Conv.%) = (weight of the produced polymer/weight of monomer) × 100.

3.6. Characterization of Polymethyl Methacrylate

Molecular weight distribution analysis of the produced polymer was carried out through gel permeation chromatography (GPC). The measurements were performed in toluene of HPLC grade with a rate of elution 0.7 mL/min at 40 °C. Monodisperse polystyrene standards were used as the reference to calculate the molecular weights of PMMA. Calculations were carried out using the Millennium 32 Chromatography Manager with the software for gel-permeation application. Proton nuclear magnetic resonance spectroscopy (¹HNMR) was used for the tacticity analysis of PMMA which was done on a Bruker-300 MHz spectrometer with a superconducting magnet and a 5 mm dual-probe head. The internal reference was tetramethylsilane and CDCl₃ was used as the solvent. The triads% (rr, mm, and rm) sequences were calculated using the following equation as an example: (rr) % = [the area under the peak of (rr) triads/the total area under the peaks of (rr + mr + mm)] × 100.

4. Conclusions

A series of catalysts based on magnetic nanoparticles doped by silver (Ag/Fe, PEI-Ag/Fe, and APTES-Ag/Fe) was prepared at room temperature using a two-step technique. The prepared nanoparticles were characterized by XRD, SEM/EDX, DLS, FT-IR, and TEM. Their activity was tested using bulk and solution polymerization conditions for MMA at 80 °C under different conditions. The produced polymer was characterized using GPC and ¹HNMR. The optimum conditions thus determined are: catalyst/benzoyl peroxide ratio 4/1 at 80 °C for 5 h and without oxygen. The results indicated that the studied Fe-based catalysts have ferrocene like behavior in MMA polymerization. Oxygen inhibits the catalyst but NaHSO₃, benzoyl peroxide and silver enhance the redox process and improve the Conv.% of PMMA.

Author Contributions: Conceptualization, S.M.S. and M.S.A.D.; Formal analysis, S.M.S. and M.S.A.D.; Methodology, S.M.S. and M.S.A.D.; Supervision, J.Y.; Writing—original draft, S.M.S. and M.S.A.D.; Writing—review & editing, J.Y. All authors have read and agreed to the published version of the manuscript.

Funding: This research was supported by the National Research Foundation (NRF) of Korea (2019M3C1B8090798), the Korea Evaluation Institute of Industrial Technology (KEIT) grant (No. 20003822), and the Korea Health Industry Development Institute (KHIDI) grant (number: HI19C1234) and Jungwon Yoon contributed equally to this work as corresponding author. The authors acknowledge the help provided by AmreEizad in the writing of this paper.

Conflicts of Interest: The authors declare no conflict of interest.

References

1. Semaltianos, N.G. Spin-coated PMMA films. *Microelectron. J.* **2007**, *38*, 754–761. [[CrossRef](#)]
2. Ikemura, K.; Endo, T. A review of our development of dental adhesives—effects of radical polymerization initiators and adhesive monomers on adhesion. *Dent. Mater. J.* **2010**, *29*, 109–121. [[CrossRef](#)] [[PubMed](#)]
3. Umar Ali, U.; Abd Karim, K.; Buang, N. A Review of the Properties and Applications of Poly (Methyl Methacrylate) (PMMA). *Polym. Rev.* **2015**, *55*, 678–705.
4. Suzuki, Y.; Cousins, D.; Wassgren, J.; Kappes, B.B.; Dorgan, J.; Stebner, A.P. Kinetics and temperature evolution during the bulk polymerization of methyl methacrylate for vacuum-assisted resin transfer molding. *Compos. Part A Appl. Sci. Manuf.* **2018**, *104*, 60–67. [[CrossRef](#)]
5. van Rijswijk, K.; Bersee, H.E.N. Reactive processing of textile fiber-reinforced thermoplastic composites—An overview. *Compos. Part A Appl. Sci. Manuf.* **2007**, *38*, 666–681. [[CrossRef](#)]
6. Monakov, Y.B.; Islamova, R.M.; Frizen, A.K.; Golovochesova, O.I.; Nazarova, S.V. Radical polymerization of methyl methacrylate in the presence of benzoyl peroxide, ferrocene and zirconocene dichloride. *Mendeleev Commun.* **2011**, *21*, 206–208. [[CrossRef](#)]
7. Al-Khalidi, U.K.; Al-Lami, H.S. Ferrocene as Accelerator for Free Radical Copolymerization of Methyl Methacrylate/Methacrylic Acid Monomers. *Iraqi J. Polym.* **2015**, *18*, 65–70.
8. Sadek, E.; Mekewi, M.; Yehia, F.; Solyman, S. Catalytic Polymerization of Methyl Methacrylate in Different Media Using Supported Metal Phthalocyanines, 1. Bulk Polymerization in Relation to the Microcrystalline Structure of Supported Metal Phthalocyanines. *Macromol. Chem. Phys.* **2001**, *202*, 1505–1512. [[CrossRef](#)]
9. Achilias, D.S.; Sideridou, I. Study of the effect of two BPO/amine initiation systems on the free-radical polymerization of MMA used in dental resins and bone cements. *J. Macromol. Sci. Part A Pure Appl. Chem.* **2002**, *39*, 1435–1450. [[CrossRef](#)]
10. Suzuki, Y.; Cousins, D.; Shinagawa, Y.; Bell, R.; Matsumoto, A.; Stebner, A. Phase separation during bulk polymerization of methyl methacrylate. *Polym. J.* **2019**, *51*, 423–431. [[CrossRef](#)]
11. Achilias, D.; Sideridou, I. Kinetics of the Benzoyl Peroxide/Amine Initiated Free-Radical Polymerization of Dental Dimethacrylate Monomers: Experimental Studies and Mathematical Modeling for TEGDMA and Bis-EMA. *Macromolecules* **2004**, *37*, 4254–4265. [[CrossRef](#)]
12. Kim, K.; Singstock, N.; Childress, K.; Sinha, J.; Salazar, A.; Whitfield, S.; Holder, A.; Stansbury, J.; Musgrave, C. Rational Design of Efficient Amine Reductant Initiators for Amine–Peroxide Redox Polymerization. *J. Am. Chem. Soc.* **2019**, *141*, 6279–6291. [[CrossRef](#)] [[PubMed](#)]
13. Zoller, A.; Gignes, D.; Guillaneuf, Y. Simulation of radical polymerization of methyl methacrylate at room temperature using a tertiary amine/BPO initiating system. *Polym. Chem.* **2015**, *6*, 5719–5727. [[CrossRef](#)]
14. Moad, G.; Solomon, D.H. *The Chemistry of Free Radical Polymerization*; Pergamon Press: Oxford, UK, 1995; pp. 72–73.
15. Han, B.; Choi, N.; Kim, K.H.; Lim, D.W.; Choo, J. Application of Silver-Coated Magnetic Microspheres to a SERS-Based Optofluidic Sensor. *J. Phys. Chem. C* **2011**, *115*, 6290–6296. [[CrossRef](#)]
16. Chatzipavlidis, A.; Bilalis, P.; Tziveleka, L.A.; Boukos, N.; Charitidis, C.A.; Kordas, G. Nanostructuring the Surface of Dual Responsive Hollow Polymer Microspheres for Versatile Utilization in Nanomedicine-Related Applications. *Langmuir* **2013**, *29*, 9562–9572. [[CrossRef](#)]
17. Venkateswarlu, S.; Kumar, B.N.; Prathima, B.; Anitha, K.; Jyothi, N.V.V. A novel green synthesis of Fe₃O₄-Ag core shell recyclable nanoparticles using Vitisvinifera stem extract and its enhanced antibacterial performance. *Phys. B Condens. Matter* **2015**, *457*, 30–35. [[CrossRef](#)]
18. Hilal, I.H.; Mohammed, M.R.; Shakir, W.A. Effect of Silver (Ag) Nanoparticles on Structural and Mechanical Properties of (PMMA) Blend and its Application for Denture Base. *Int. J. Med. Res. Health Sci.* **2019**, *8*, 154–159.
19. Zhou, S.; Chen, Q. Synthesis and characterization of bracelet-like magnetic nanorings consisting of Ag–Fe₃O₄ bi-component nanoparticles. *Dalton Trans.* **2011**, *40*, 8622–8629. [[CrossRef](#)]
20. Brollo, M.F.; López-Ruiz, R.; Muraca, D.; Figueroa, S.A.; Pirota, K.R.; Knobel, M. Compact Ag@Fe₃O₄ Core-shell Nanoparticles by Means of Single-step Thermal Decomposition Reaction. *Sci. Rep.* **2015**, *4*, 6839. [[CrossRef](#)]
21. Darwish, M.S.A.; Kunz, U.; Peuker, U. Preparation and catalytic use of platinum in magnetic core/shell nanocomposites. *J. Appl. Polym. Sci.* **2013**, *129*, 1806–1811. [[CrossRef](#)]

22. Polshettiwar, V.; Luque, R.; Fihri, A.; Zhu, H.; Bouhrara, M.; Basset, J. Magnetically Recoverable Nanocatalysts. *Chem. Rev.* **2011**, *111*, 3036–3075. [[CrossRef](#)] [[PubMed](#)]
23. Sankar, M.; Dimitratos, N.; Miedziak, P.; Wells, P.; Kiely, C.; Hutchings, G. Designing bimetallic catalysts for a green and sustainable future. *Chem. Soc. Rev.* **2012**, *41*, 8099–8139. [[CrossRef](#)] [[PubMed](#)]
24. Shokouhimehr, M. Magnetically Separable and Sustainable Nanostructured Catalysts for Heterogeneous Reduction of Nitroaromatics. *Catalysts* **2015**, *5*, 534–560. [[CrossRef](#)]
25. Shifrina, Z.; Bronstein, L. Magnetically Recoverable Catalysts: Beyond Magnetic Separation. *Front. Chem.* **2018**, *6*, 298. [[CrossRef](#)] [[PubMed](#)]
26. Zhang, X.; Jiang, W.; Zhou, Y.; Xuan, S.; Peng, C.; Zong, L.; Gong, X. Magnetic recyclable Ag catalysts with a hierarchical nanostructure. *Nanotechnology* **2011**, *22*, 375701. [[CrossRef](#)] [[PubMed](#)]
27. Chen, M.; Zheng, X. Catalyst characterization and surface oxygen properties of Ag-Fe mixed oxide catalysts. *Indian J. Chem.* **2001**, *40A*, 298–302.
28. Jodaei, A.; Niaei, A.; Salari, D. Performance of nanostructure Fe-Ag-ZSM-5 catalysts for the catalytic oxidation of volatile organic compounds: Process optimization using response surface methodology. *Korean J. Chem. Eng.* **2011**, *28*, 1665–1671. [[CrossRef](#)]
29. Gupta, V.; Yola, M.; Eren, T.; Kartal, F.; Çağlayan, M.; Atar, N. Catalytic activity of Fe@Ag nanoparticle involved calcium alginate beads for the reduction of nitrophenols. *J. Mol. Liq.* **2014**, *190*, 133–138. [[CrossRef](#)]
30. Chou, K.; Lin, M.; Wu, H. Studies on the removal of 2-propanol by Ag@Fe₂O₃ core-shell structured catalyst. *J. Taiwan Inst. Chem. Eng.* **2013**, *44*, 28–232. [[CrossRef](#)]
31. Biabani-Ravandi, A.; Rezaei, M.; Fattah, Z. Catalytic performance of Ag/Fe₂O₃ for the low temperature oxidation of carbon monoxide. *Chem. Eng. J.* **2013**, *219*, 124–130. [[CrossRef](#)]
32. Vural, M.; Crowgey, B.; Kempel, L.; Kofinas, P. Nanostructured flexible magneto-dielectrics for radio frequency applications. *J. Mater. Chem. C* **2014**, *2*, 756–763. [[CrossRef](#)]
33. Amarjargal, A.; Tijing, L.D.; Im, I.T.; Kim, C.S. Simultaneous preparation of Ag/Fe₃O₄ core-shell nanocomposites with enhanced magnetic moment and strong antibacterial and catalytic properties. *Chem. Eng. J.* **2013**, *226*, 243–254. [[CrossRef](#)]
34. Chudasama, B.; Vala, A.K.; Andhariya, N.; Upadhyay, R.V.; Mehta, R.V. Antifungal activity of multifunctional Fe₃O₄-Ag nanocolloids. *J. Magn. Magn. Mater.* **2011**, *323*, 1233–1237. [[CrossRef](#)]
35. Lopes, G.; Vargas, J.; Sharma, S.; Béron, F.; Pirota, K.; Knobel, K.; Rettori, C.; Zysler, R. Ag-Fe₃O₄ Dimer Colloidal Nanoparticles: Synthesis and Enhancement of Magnetic Properties. *J. Phys. Chem. C* **2010**, *114*, 10148–10152. [[CrossRef](#)]
36. Sun, Y.; Li, X.; Cao, J.; Zhang, W.; Wang, H. Characterization of zero-valent iron nanoparticles. *Adv. Colloid Interface Sci.* **2006**, *120*, 47–56. [[CrossRef](#)]
37. Liang, W.; Dai, C.; Zhou, X.; Zhang, Y. Application of Zero-Valent Iron Nanoparticles for the Removal of Aqueous Zinc Ions under Various Experimental Conditions. *PLoS ONE* **2014**, *9*, e85686. [[CrossRef](#)]
38. Chaki, S.; Malek, T.; Chaudhary, M.; Tailo, J.; Deshpande, M. Magnetite Fe₃O₄ nanoparticles synthesis by wet chemical reduction and their characterization. *Adv. Nat. Sci. Nanosci. Nanotechnol.* **2015**, *6*, 035009. [[CrossRef](#)]
39. Mukhtar, A.; Cao, X.; Mehmood, T.; Wang, D.; Wu, K. Structural characterization of self-assembled chain like Fe-FeOx Core shell nanostructure. *Nanoscale Res. Lett.* **2019**, *14*, 308. [[CrossRef](#)]
40. Lee, H.; Lee, S.; Oh, E.; Chung, H.; Han, S.; Kim, E.; Seo, S.; Ghim, H.; Yeum, J.; Choi, J. Antimicrobial polyethyleneimine-silver nanoparticles in a stable colloidal dispersion. *Colloids Surf. B Biointerfaces* **2011**, *88*, 505–511. [[CrossRef](#)]
41. Lim, J.; Yeap, S.; Che, H.; Low, S. Characterization of magnetic nanoparticle by dynamic light scattering. *Nanoscale Res. Lett.* **2013**, *8*, 381. [[CrossRef](#)]
42. Darwish, M.S.A.; El-Sabbagh, A.; Stibor, I. Hyperthermia properties of magnetic polyethylenimine core/shell nanoparticles: Influence of carrier and magnetic field strength. *J. Polym. Res.* **2015**, *22*, 1–6. [[CrossRef](#)]
43. Takahashi, K.; Kato, H.; Saito, T.; Matsuyama, S.; Kinugasa, S. Precise measurement of the size of nanoparticles by dynamic light scattering with uncertainty analysis. *Part. Part. Syst. Charact.* **2008**, *8*, 31–38. [[CrossRef](#)]
44. Darwish, M.S.A.; Stibor, I. Preparation and characterization of magnetite-PDMS composites by magnetic induction heating. *Mater. Chem. Phys.* **2015**, *164*, 163–169. [[CrossRef](#)]
45. Hurvois, J.P.; Moinet, C. Reactivity of ferrocenium cations with molecular oxygen in polar organic solvents: Decomposition, redox reactions and stabilization. *J. Organomet. Chem.* **2005**, *690*, 1829–1839. [[CrossRef](#)]

46. Jenjob, S.; Tharawut, T.; Sunintaboon, P. Facile synthesis of silver immobilized-poly(methyl methacrylate)/polyethyleneimine core-shell particle composites. *Mater. Sci. Eng. C* **2012**, *32*, 2068–2072. [[CrossRef](#)]
47. Pimpha, N.; Chaleawlert-umpon, S.; Sunintaboon, P. Core/shell polymethyl methacrylate/polyethyleneimine particles incorporating large amounts of iron oxide nanoparticles prepared by emulsifier-free emulsion polymerization. *Polymer* **2012**, *53*, 2015–2022. [[CrossRef](#)]
48. Chiu, T.; Don, T. Synthesis and characterization of poly(methyl methacrylate) nanoparticles by emulsifier-free emulsion polymerization with a redox-initiated system. *J. Appl. Polym. Sci.* **2008**, *109*, 3622–3630. [[CrossRef](#)]
49. Islamova, R.M. Iron Compounds in Controlled Radical Polymerization: Ferrocenes, (Clathro)chelates, and Porphyrins. *Russ. J. Gen. Chem.* **2016**, *86*, 125–143. [[CrossRef](#)]
50. Murinov, Y.; Grabovskiy, S.; Islamova, R.; Kuramshina, A.N.; Kabal'nova, N. Mechanism of Methyl Methacrylate Polymerization Initiated by Benzoyl Peroxide and Ferrocene in the Presence of Oxygen. *Mendeleev Commun.* **2013**, *23*, 53–55. [[CrossRef](#)]
51. Andriyashina, N.M.; Grabovskii, S.A.; Kabal'nova, N.N. Decomposition of Benzoyl Peroxide in the Presence of Ferrocene. *Russ. J. Gen. Chem.* **2019**, *89*, 1560–1563. [[CrossRef](#)]
52. Kalenda, P.; Jarusek, J. Accelerating effects of ferrocene in polymerization reactions. *Chem. Pap.* **1991**, *45*, 119–125.
53. Solyman, S.M.; Azzam, E.M.S.; Sayyah, S.M. The performance of modified nanoclay using polymeric thiol surfactants assembled on gold nanoparticles in heterogeneous bulk polymerization of methyl methacrylate. *Appl. Catal. A Gen.* **2014**, *475*, 218–225. [[CrossRef](#)]



© 2020 by the authors. Licensee MDPI, Basel, Switzerland. This article is an open access article distributed under the terms and conditions of the Creative Commons Attribution (CC BY) license (<http://creativecommons.org/licenses/by/4.0/>).